nature astronomy

SUPPLEMENTARY INFORMATION

https://doi.org/10.1038/s41550-019-0772-5

In the format provided by the authors and unedited.

Time variation of Jupiter's internal magnetic field consistent with zonal wind advection

K. M. Moore[1*], H. Cao[1,2], J. Bloxham[1], D. J. Stevenson[2], J. E. P. Connerney[3,4] and S. J. Bolton[5]

[1]Department of Earth and Planetary Sciences, Harvard University, Cambridge, MA, USA. [2]Division of Geological and Planetary Sciences, California Institute of Technology, Pasadena, CA, USA. [3]Space Research Corporation, Annapolis, MD, USA. [4]NASA Goddard Space Flight Center, Greenbelt, MD, USA. [5]Southwest Research Institute, San Antonio, TX, USA. *e-mail: kimberlymoore@g.harvard.edu

Supporting Information

Time-variation of Jupiter's internal magnetic field consistent with zonal wind advection

K. M. Moore[1], H. Cao[1], J. Bloxham[1], D. J. Stevenson[2], J. E. P. Connerney[3,4], and S. J. Bolton[5]

[1]Department of Earth & Planetary Sciences, Harvard University, Cambridge MA 02138, USA

[2]Division of Geological and Planetary Sciences, California Institute of Technology, Pasadena, CA 91125, USA

[3]NASA Goddard Spaceflight Center, Greenbelt, MD 20771, USA

[4]Space Research Corporation, Annapolis, MD 21403, USA

[5]Southwest Research Institute, San Antonio, TX 78238, USA

Introduction

This supporting information contains additional details on the modeling performed in the main text, and spherical harmonic coefficients for our zonal wind advection (ZWA) model. Specifically, we enclose a figure (Supplementary Figure 1) demonstrating our external field models and fit to the data, and the parameters used therein (Supplementary Table 1); a figure showing the effect of alternative rotation periods on the enclosed secular variation (Supplementary Figure 2); a comparison of Jovian rotation periods between several published studies (Supplementary Table 2); a figure showing the fit of our ZWA model to the inferred secular variation for an alternative rotation period (Supplementary Figure 3); a figure showing Jupiter's zonal winds projected to alternative projection depths (Supplementary Figure 4); a figure showing the fit to the inferred secular variation using alternative wind projection depths (Supplementary Figure 5); and a figure showing the relative magnitude of each error source for the past spacecraft magnetometer data used in our study (Supplementary Figure 6).

We also enclose a list of spherical harmonic coefficients for our ZWA (zonal wind advection) model of Jupiter's secular variation using zonal winds projected to 0.95RJ (Supplementary Dataset 1), 0.94 RJ (Supplementary Dataset 2), and 0.93 RJ (Supplementary Dataset 3). These datasets are in ASCII format.

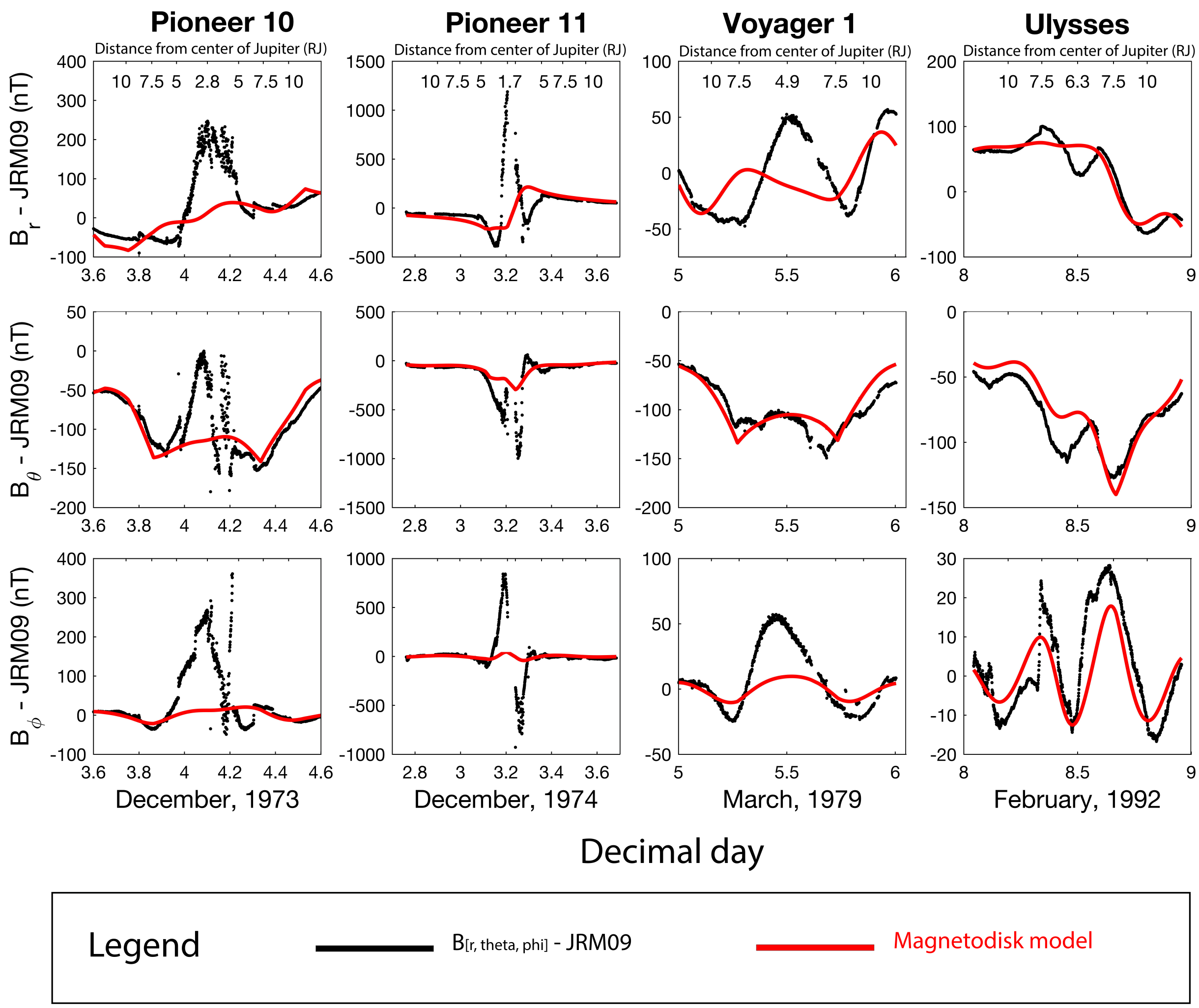

Supplementary Figure 1. Fitting the magnetodisk model. This plot compares the fit of our magnetodisk models (red, calculated based off of Connerney et al., 1981) to the observed magnetic field data minus JRM09 (Connerney et al., 2018; black).

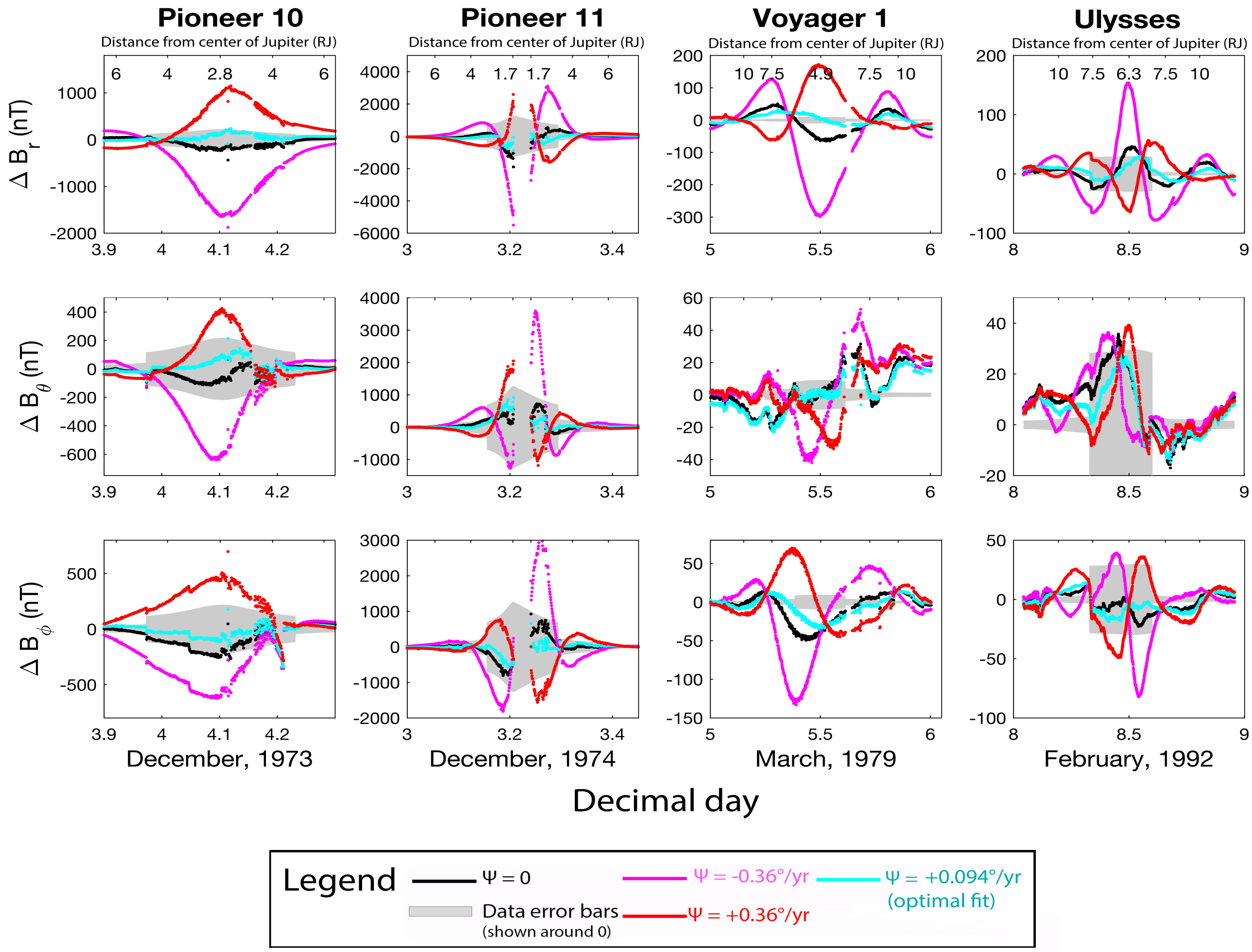

Supplementary Figure 2. Comparing alternative rotation periods. We show how the inferred secular variation depends on Jupiter's rotation period. We show the change in magnetic field (y-axis) between Juno and past spacecraft missions along the spacecraft flight path (x-axis), for the r-, theta-, and phi-components (top, middle, and bottom respectively). We plot: the slowest and fastest rotation periods within the System III (1965) uncertainty bounds (respectively Ψ = -0.36 deg/yr, magenta; and Ψ = +0.36 deg/yr, red); the standard System III (1965) rotation period (Ψ = 0, black); and the rotation period that minimizes the inferred secular variation across the four missions (Ψ = +0.094 deg/yr, cyan). Since no rotation period reduces Delta B to zero (within data error bounds) for all missions, a rotation period is not enough to explain the inferred secular variation in Jupiter's magnetic field.

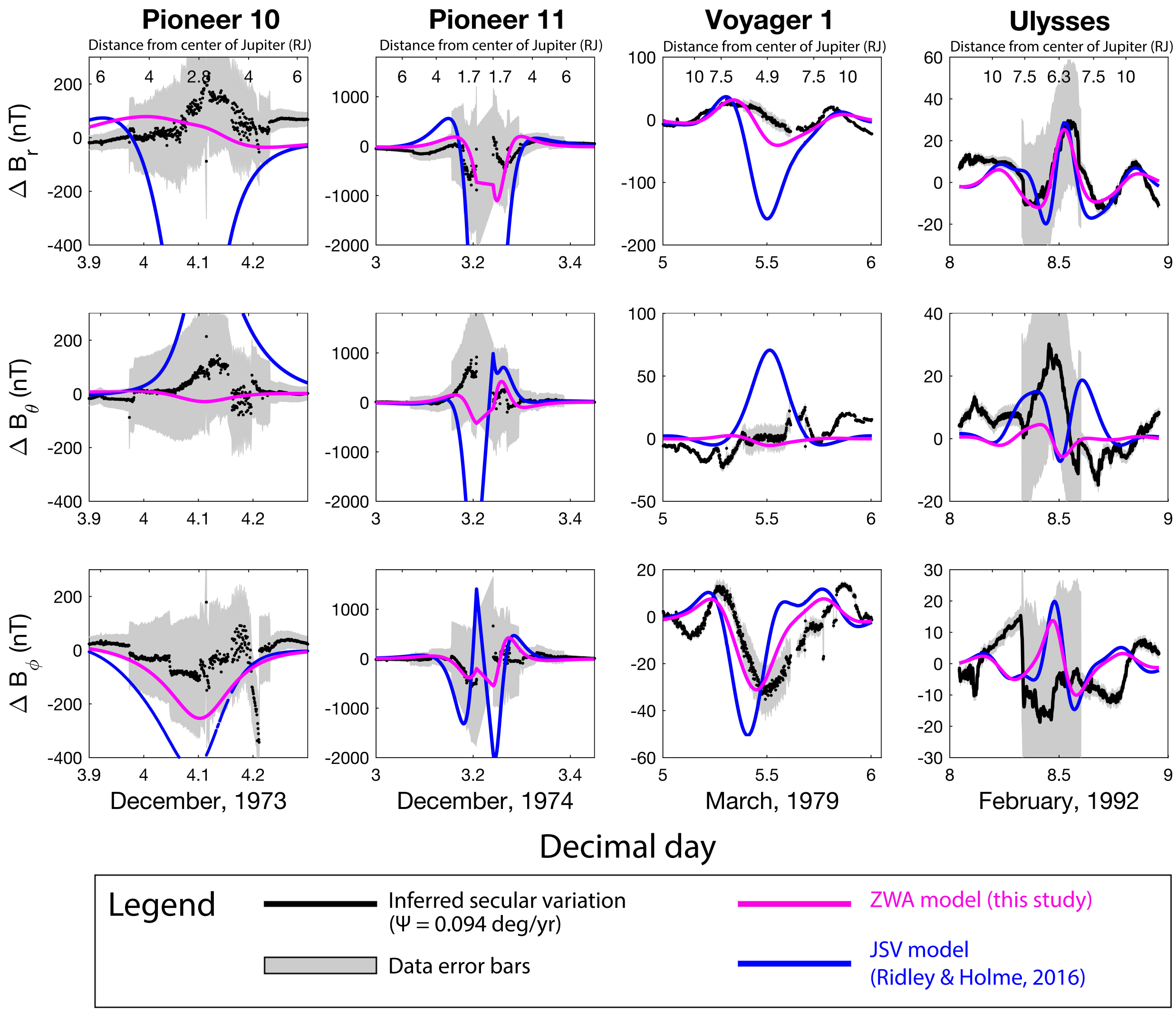

Supplementary Figure 3. Models of Jupiter's magnetic secular variation using an alternative Jovian rotation period We compare models of Jupiter's secular variation (JSV [Ridley & Holme, 2016] in blue, and ZWA [this study] in magenta), to the actual inferred change in Jupiter's internal magnetic field between Juno and past spacecraft missions (black), where the coordinates have been adjusted using a coordinate system drift rate of Ψ = 0.094 deg/yr (see Methods for details). The shaded grey region denotes the measurement error bars (see Methods for calculation details). For this figure, we use a magnetic drift rate of 0.025 m/s for the ZWA model, instead of 0.0375 m/s. This is because some of the apparent drift of magnetic features could be accommodated by a rotation period change (longitude shift) in the coordinate system, instead of advection by zonal winds.

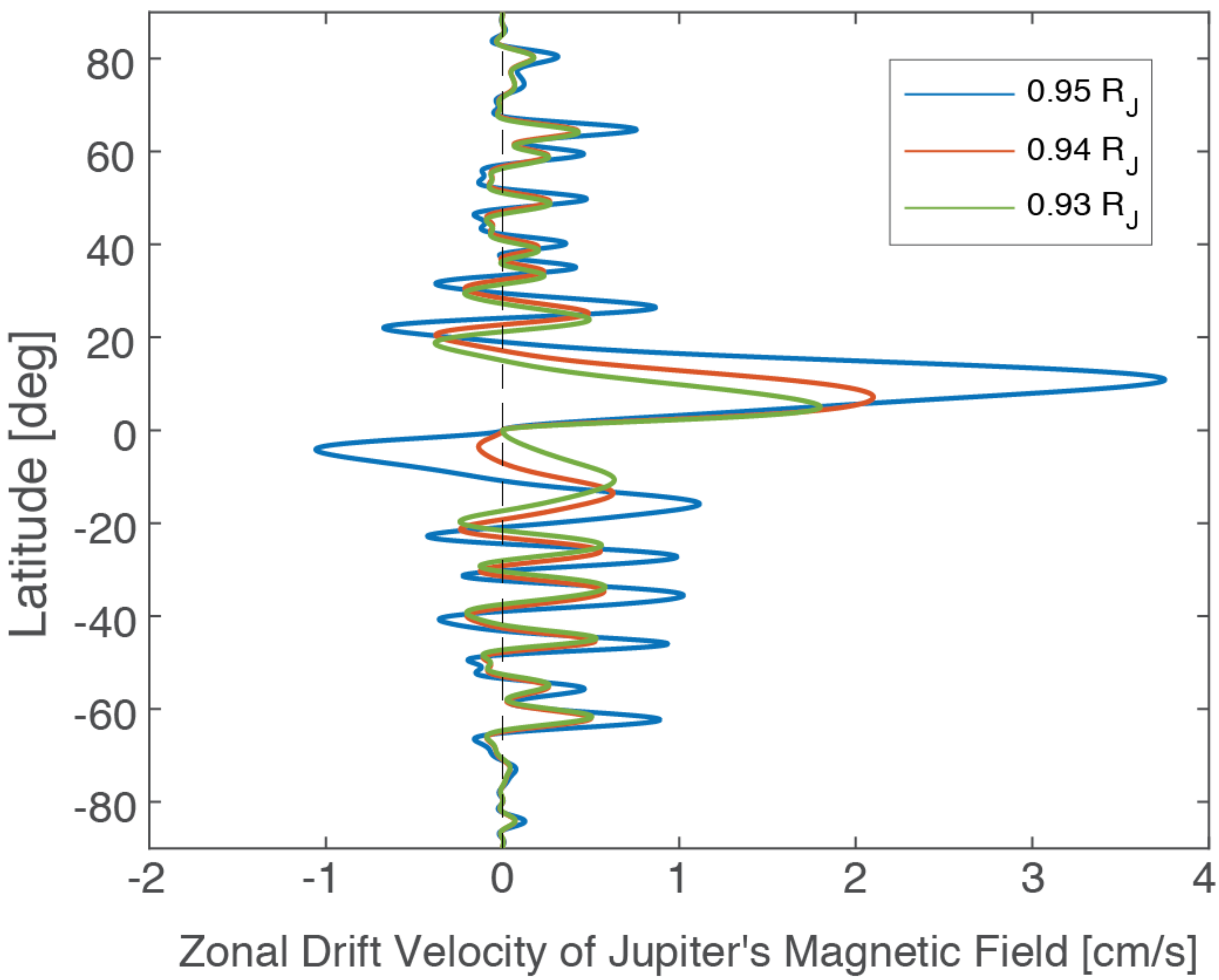

Supplementary Figure 4. Zonal wind geometry using alternative projection depths Here we show the wind geometries that result when projecting Jupiter's surface winds to depths of 0.93 (green), 0.94 (orange), and 0.95 RJ (blue), and scaling the peak amplitude to 1.8 cm/s, 2.1 cm/s, and 3.75 cm/s respectively.

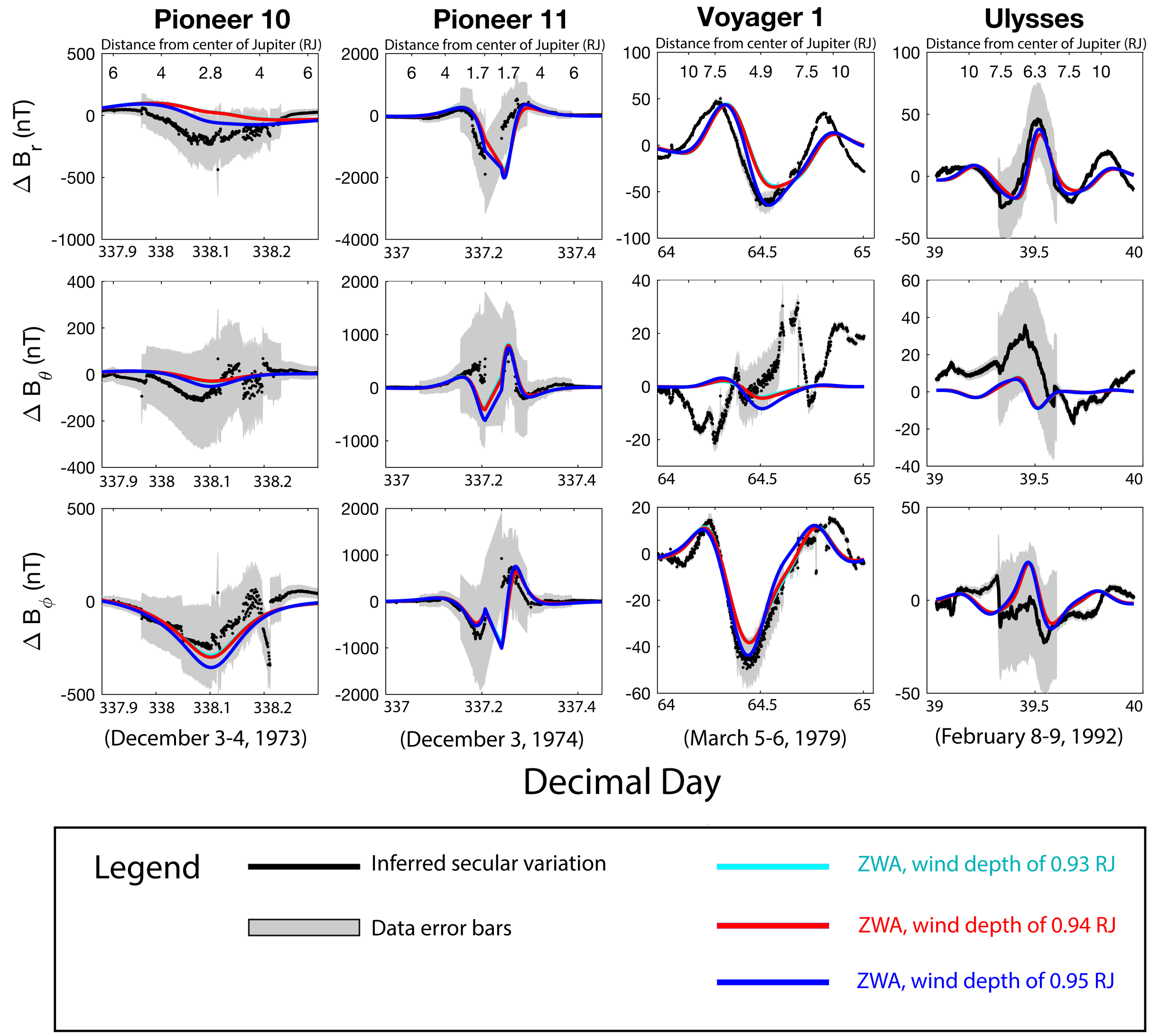

Supplementary Figure 5. Comparing alternative wind depths Here we show the fit of our ZWA model to the inferred change in Jupiter's internal magnetic field between Juno and past spacecraft missions (black). The shaded grey region denotes the measurement error bars, shown here bracketing the inferred secular variation (see Methods in main text for calculation details). We show ZWA models calculated by projecting Jupiter's surface winds to three different depths (see Figure S4): 0.93 RJ (cyan), 0.94 RJ (red), and 0.95 RJ (royal blue). The 0.93 RJ and 0.94 RJ models plot nearly on top of each other. The 0.95 RJ model shown here is the same ZWA model that is shown in the main text.

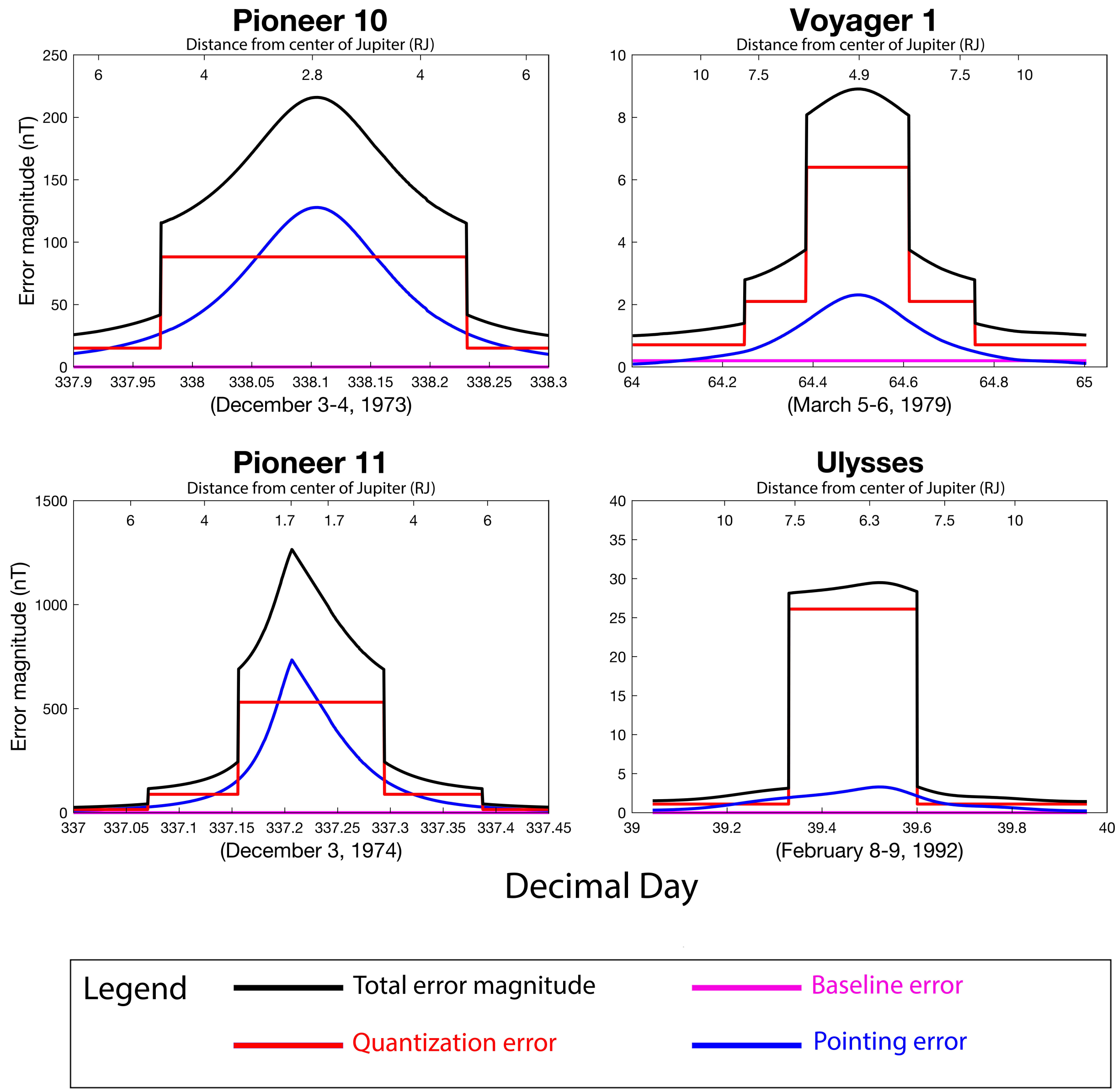

Supplementary Figure 6. Comparison of magnetometer data error magnitudes by source for past spacecraft missions Here we show the relative contribution of each error source (baseline sensor accuracy in magenta, data quantization error in red, and pointing error in blue) to the total error source (black line) along the spacecraft flight track for Pioneer 10, Pioneer 11, Voyager 1, and Ulysses.

We assume the pointing error is an arbitrary rotation about the spacecraft's presumed orientation and take an order of magnitude estimate, rather than modeling it component by component. In reality, the errors are likely anisotropic. For example, consider the case of a magnetic field **B** = (0,0,B) measured in the spacecraft frame (x,y,z). If the assumed attitude was wrong by a small rotation angle α relative to the z axis, then the field transform between spacecraft coordinates and a reference coordinate system (such as System III) will lead to errors of (1-cos(α))B in Bz, and sin(α)B in the field perpendicular to the z axis (approximately $-0.5\alpha^2 B$ and α respectively for small angles). See Holme & Bloxham (1996) for a full treatment of anisotropic attitude errors in spacecraft data analysis.

Supplementary Table 1. Magnetodisk parameters from Monte Carlo analysis.

Parameter	**Value**			
	Pioneer 10	**Pioneer 11**	**Voyager 1**	**Ulysses**
R_0	7.22 RJ	3.04 RJ	7.65 RJ	7.66 RJ
D	3.47 RJ	2.82 RJ	2.52 RJ	3.42 RJ
$\mu_0 I$	282.0	367.7	345.8	292.2
θ	9.6 deg	9.7 deg	5.3 deg	7.7 deg
φ	254.1 deg	254.1 deg	208.2 deg	283.7 deg

This table shows the magnetodisk parameters for our ZWA model using winds projected to 0.95RJ. Here θ is the dipole tilt, and φ is the dipole londitude. R1 was kept constant at 50 RJ (Jupiter radii). These parameters assume the standard System III (1965) Jovian rotation period, and correspond to the 6-parameter model described in Connerney et al. (1981).

Supplementary Table 2. Comparison of Jovian rotation rate studies

Reference	**Rotation period**	Coordinate system drift rate, **Ψ** (deg/yr)
System III (1965)	9h 55min 29.711 +/- 0.04 sec	N/A
Higgins et al. (1997)	9h 55min 29.6854 +/- 0.0035 sec	-0.23
Russell et al. (2001)	9h 55min 29.710 sec	-0.0089
Ridley & Holme (2016)	9h 55min 29.7258 sec	+0.13
This study:		
Pioneer 10 optimal fit	9h 55min 29.718 sec	+0.069
Pioneer 11 optimal fit	9h 55min 29.722 sec	+0.096
Voyager 1 optimal fit	9h 55min 29.723 sec	+0.11
Ulysses optimal fit	9h 55min 29.723 sec	+0.11

We convert the rotation periods published in other studies to a variety of units for ease of comparison. The drift rates (Psi) are given with reference to 2017.0:

$\phi' = \phi + \Psi*(2017-t)$

Where ϕ' is the rotated E longitude in the new coordinate system, ϕ is the original datapoint E longitude, Ψ is the coordinate system drift rate in deg/yr, and t is the datapoint decimal year.

With this set of definitions, 2017.0 is taken as the reference date for our rotated coordinate systems, and has an equivalent longitude to System III (1965). Positive drift rates indicate increasing East longitudes before 2017, and decreasing E longitudes after 2017 (a slower rotation period), and negative drift rates indicate a faster rotation period. Coordinates at 2017.0 will be unchanged.

Supplementary Dataset 1. This dataset contains spherical harmonic coefficients for our zonal wind advection (ZWA) model using winds projected to 0.95 RJ**,** in nT/yr. We use RJ = 71492km and a drift rate of 3.75 cm/s. To calculate the coefficients for a different field drift rate, simply multiply them by a scalar (e.g. multiply current values by 2 for a drift rate of 7.5 cm/s). The coefficients appear in the following order: g10, g11, h11, g20, g21, h21, g22, etc.

Supplementary Dataset 2. This dataset **contains spherical harmonic coefficients for** our zonal wind advection (ZWA) model using winds projected to 0.94 RJ**,** in nT/yr. We use RJ = 71492km and a drift rate of 2.1 cm/s. To calculate the coefficients for a different field drift rate, simply multiply them by a scalar (e.g. multiply current values by 2 for a drift rate of 4.2 cm/s). The coefficients appear in the following order: g10, g11, h11, g20, g21, h21, etc.

Supplementary Dataset 3. This dataset contains spherical harmonic coefficients for our zonal wind advection (ZWA) model using winds projected to 0.93 RJ**,** in nT/yr. We use RJ = 71492km and a drift rate of 1.8 cm/s. To calculate the coefficients for a different field drift rate, simply multiply them by a scalar (e.g. multiply current values by 2 for a drift rate of 3.6 cm/s). The coefficients appear in the following order: g10, g11, h11, g20, g21, h21, g22, etc.

References:

Connerney, J. E. P., Acuña, M. H., and Ness, F. (1981). Modeling the Jovian current sheet and inner magnetosphere. *Journal of Geophysical Research*, 86, A10, 8370-8384.

Connerney, J. E. P., Acuña, M. H., and Ness, F. (1984). The Z3 model of Saturn's magnetic field and the Pioneer 11 vector helium magnetometer observations. *Journal of Geophysical Research 89*, A9, 7541-7544.

Edwards, T. M., Bunce, E. J., and Cowley, S. W. H. (2001). A note on the vector potential of Connerney et al.'s model of the equatorial current sheet in Jupiter's magnetosphere. *Planetary and Space Science* 49, 10-11, 1115-1123.

Higgins, C. A., Carr, T. D., Reyes, F., Greenman, W. B., and Lebo, G. R. (1997). A redefinition of Jupiter's rotation period. *Journal of Geophysical Research,* 102, A10, 22033-22041.

Holme, R. and Bloxham, J. (1996). The treatment of attitude errors in satellite geomagnetic data. *Physics of the Earth and Planetary Interiors 98*, 221-233.

Ridley, V. A., and Holme, R. (2016). Modeling the Jovian magnetic field and its secular variation using all available magnetic field observations. *Journal of Geophysical Research*, 121, 309-337.

Russell, C. T., Yu, Z., and Kivelson, M. G. (2001). The rotation period of Jupiter. *Geophysical Research Letters*, 28, 10, 1911-1912.

Smith, E.J., Davis Jr., L., Jones, D. E., Coleman Jr., Colburn, D. S., Dyal, P., Sonett, C. P., and Frandsen, A. M. A. (1974). The planetary magnetic field and magnetosphere of Jupiter: Pioneer 10. *Journal of Geophysical Research 79, 25, 3501-3513.*